THE ASTROPHYSICAL JOURNAL, 464:L25–L28, 1996 June 10

TWO-POINT CORRELATIONS IN THE *COBE*[1] DMR FOUR-YEAR ANISOTROPY MAPS

G. HINSHAW,[2,3] A. J. BANDAY,[2,4] C. L. BENNETT,[5] K. M. GÓRSKI,[2,6] A. KOGUT,[2] C. H. LINEWEAVER,[7] G. F. SMOOT,[8] AND E. L. WRIGHT[9]
Received 1996 January 9; accepted 1996 March 21

ABSTRACT

The two-point temperature correlation function is evaluated from the 4 yr *COBE* DMR microwave anisotropy maps. We examine the two-point function, which is the Legendre transform of the angular power spectrum, and show that the data are statistically consistent from channel to channel and frequency to frequency. The most likely quadrupole normalization is computed for a scale-invariant power-law spectrum of CMB anisotropy, using a variety of data combinations. For a given data set, the normalization inferred from the two-point data is consistent with that inferred by other methods. The smallest and largest normalizations deduced from any data combination are 16.4 and 19.6 μK, respectively, with a value $\sim$18 μK generally preferred.

Subject headings: cosmic microwave background — cosmology: observations

1. INTRODUCTION

The detection of large angular scale anisotropies in the cosmic microwave background (CMB) radiation was first reported by the *COBE* DMR experiment in 1992 (Smoot et al. 1992; Bennett et al. 1992; Wright et al. 1992; Kogut et al. 1992). The initial detection was based only on the first year of flight data. Since that time the DMR team processed and analyzed the first 2 yr of data and found the results to be consistent with the first year results (Bennett et al. 1994; Górski et al. 1994; Wright et al. 1994a). We have now processed and analyzed the full 4 yr of DMR observations: this paper is one of a series describing the results of our analysis. The maps and an overview of the scientific results are given in Bennett et al. (1996).

In this paper we analyze the anisotropy in the 4 year DMR maps using the two-point correlation function as a measure of the angular power spectrum. The *COBE* DMR experiment was designed to measure the CMB anisotropy on angular scales of $\geq$7°, corresponding to spherical harmonic multipole moments of order $\ell \lesssim 30$. The DMR has produced full-sky maps of the CMB temperature at each of three frequencies, 31.5, 53, and 90 GHz, with two independent channels, A and B, at each frequency. In principle, one can obtain an estimate of the CMB power spectrum from an anisotropy map simply by decomposing the map, $T(\theta, \phi)$, into spherical harmonic components and averaging them to find the mean power per mode ℓ: $T(\theta, \phi) = \sum_{\ell,m} a_{\ell m} Y_{\ell m}(\theta, \phi)$ with power spectrum $a_\ell^2 = (\sum_{m=-\ell}^{\ell} |a_{\ell m}|^2)/(2\ell + 1)$. In practice, however, there are a number of complications that arise. First, the need to apply a Galactic cut to the data renders the spherical harmonics nonorthogonal, thereby coupling the $a_{\ell m}$ coefficients and increasing their uncertainty. Moreover, since a_ℓ^2 is a quadratic form, any uncertainty in the $a_{\ell m}$ (whether due to coupling, instrument noise, systematic effects, and/or foreground sources) produces a positive bias in the estimate of the power spectrum. However, see Górski et al. (1996) and Wright et al. (1996) for spherical harmonic–based analyses that account for these difficulties.

An alternative to estimating the power spectrum is to evaluate its Legendre transform, the two-point correlation function. For a given power spectrum with multipole amplitudes $C_\ell = \langle |a_{\ell m}|^2 \rangle$, the predicted covariance between pairs of map pixels i and j with angular separation α_{ij} is

$$C(\alpha_{ij}) = \langle T_i T_j \rangle = \frac{1}{4\pi} \sum_\ell (2\ell + 1) W_\ell^2 \, C_\ell \, P_\ell(\cos \alpha_{ij}), \quad (1)$$

where T_i is the CMB temperature in pixel i, the angle brackets denote an average over an ensemble of universal observers, W_ℓ is the experimental window function that includes the effects of beam smoothing and finite pixel size ($W_\ell = G_\ell F_\ell$, where the G_ℓ are the Legendre coefficients of the DMR beam pattern, tabulated by Wright et al. 1994b, and F_ℓ are the Legendre coefficients for a circular top-hat function with area equal to the pixel area; the coefficients for index level 6 pixels are available upon request), and $P_\ell(\cos \alpha_{ij})$ is the Legendre polynomial of order ℓ. We estimate the two-point correlation function in our sky by evaluating the average product of all map temperatures with a fixed angular separation, $C(\alpha) = \sum_{i,j} w_i w_j \, T_i T_j / \sum_{i,j} w_i w_j$, where the sum is restricted to pixel pairs (i, j) separated by an angle α, T_i is the observed temperature in pixel i after monopole and dipole (and optionally quadrupole) subtraction, and w_i is the statistical weight of pixel i. This statistic is straightforward to compute and offers a quick test of the consistency of the power spectrum from map to map.

In the approximation that the two-point function can be treated as a multivariate Gaussian distribution, one can form a likelihood function with which to estimate the power spectrum normalization. In § 2 we present the two-point correla-

[1] The National Aeronautics and Space Administration/Goddard Space Flight Center (NASA/GSFC) is responsible for the design, development, and operation of the *Cosmic Background Explorer* (*COBE*). Scientific guidance is provided by the *COBE* Science Working Group. GSFC is also responsible for the development of the analysis software and for the production of the mission data sets.

[2] Hughes STX Corporation, Laboratory for Astronomy and Solar Physics, Code 685, NASA/GSFC, Greenbelt, MD 20771.

[3] E-mail: hinshaw@stars.gsfc.nasa.gov.

[4] Current address: Max-Planck-Institut für Astrophysik, Karl-Swarzschild-Strasse 1, 85740 Garching bei München, Germany.

[5] Laboratory for Astronomy and Solar Physics, Code 685, NASA/GSFC, Greenbelt, MD 20771.

[6] On leave from Warsaw University Observatory, Aleje Ujazdowskie 4, 00-478 Warsaw, Poland.

[7] Observatoire de Strasbourg, 67000, Strasbourg, France.

[8] Department of Physics, Lawrence Berkeley Laboratory, Space Sciences Laboratory, and Center for Particle Astrophysics, Building 50-351, University of California, Berkeley, CA 94720.

[9] UCLA Astronomy P.O. Box 951562, Los Angeles, CA 90095-1562.

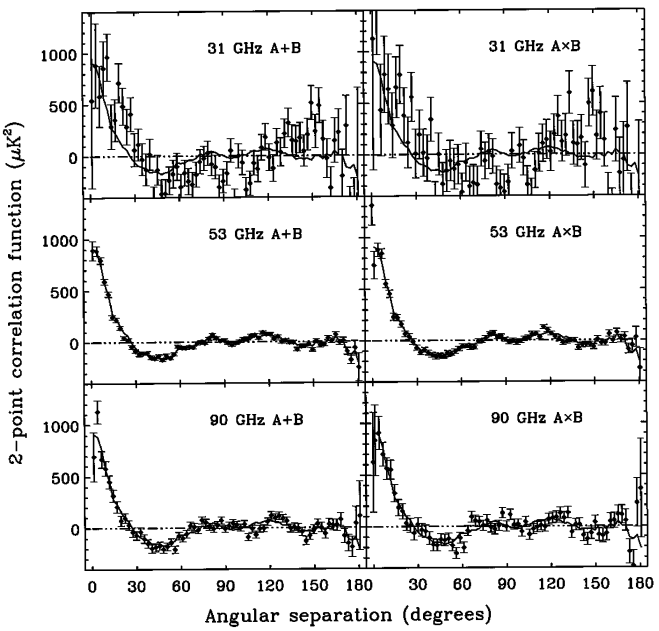

FIG. 1.—Two-point correlation functions obtained from the individual frequency maps, after monopole and dipole subtraction. Left-hand panels show the autocorrelation functions obtained from a weighted average of the A and B channel maps (the point at zero lag is off-scale due to the noise contribution). Right-hand panels show the cross-correlation of the A and B channels, which are sensitive only to common structure in the maps. Error bars represent the uncertainty due to instrument noise, as described in the text. To guide the eye, the solid line is the autocorrelation of the weighted average of all six channels maps. All six two-point functions are statistically consistent with each other.

tion data in the 4 yr DMR maps and examine its consistency from map to map. In § 3 we evaluate the Gaussian likelihood as a function of the mean expected quadrupole moment, $Q_{\rm rms-PS}$, under the assumption of a scale-invariant, power-law spectrum of anisotropy.

2. TWO-POINT CORRELATION DATA

The two-point correlation function, as given above, is the average product of all pixel temperatures with a fixed angular separation. The correlation data are binned into angular separation bins of width 2°.6 with the first bin reserved for all pixel pairs (i, j) such that $i = j$, the second bin for pairs with separation between 0° and 2°.6, and so forth; there are 71 such bins. For the present analysis we employ the maps pixelized in Galactic coordinates and use the custom Galaxy cut described by Bennett et al. (1996), for which there are 3881 surviving pixels. To minimize the total uncertainty in the two-point data, due to noise plus cosmic and sample variance, we assign equal weight to each surviving pixel, $w_i = 1$, instead of $w_i = 1/\sigma_i^2$. This has the effect of increasing the noise contribution slightly, but it *decreases* the sample variance by a slightly larger factor. Uniform weighting reduces the total uncertainty by a few percent for the 4 yr data.

The basic two-point functions obtained from the single-frequency maps are shown in Figure 1. We plot both the autocorrelation of the weighted sum of channels A and B at each frequency (the coefficients used to form the weighted average maps analyzed in this Letter are given in Table 1) and the cross-correlation between channels A and B. For reference, we also plot, as a solid line, the autocorrelation of the weighted average of all six DMR channel maps. The error bar attached to each point represents the rms due to instrument noise, based on 2000 Monte Carlo simulations that include only instrument noise. The plot clearly demonstrates excellent consistency of the two-point correlations at 53 and 90 GHz, even in the absence of any Galactic signal corrections. The 31 GHz data exhibit a small discrepancy from the mean data that is primarily quadrupolar and is presumably due to residual Galactic emission.

TABLE 1

DMR MAP COMBINATION COEFFICIENTS

Map	31A	31B	53A	53B	90A	90B
31 ws[a]	0.611	0.389	0	0	0	0
53 ws[a]	0	0	0.579	0.421	0	0
90 ws[a]	0	0	0	0	0.382	0.618
53 + 90[a]	0	0	0.412	0.299	0.110	0.179
31 + 53 + 90[a]	0.049	0.032	0.378	0.275	0.102	0.164
Correlation[b]	0.049	0.032	0.378	0.275	0.102	0.164
Combination[c]	−0.185	−0.117	0.367	0.266	0.256	0.413

[a] Maps are formed using the above coefficients according to $T = \sum_i C^i_{\rm DMR}\, T^i_{\rm DMR}$, where i = 31A, ..., 90B is a channel index, $C^i_{\rm DMR}$ are the DMR map coefficients given above, and $T_{\rm DMR}$ are the DMR maps in μK of thermodynamic temperature. The resulting map has units of μK, thermodynamic.

[b] Same as 31 + 53 + 90 except that each channel map is modified by subtracting best-fit Galactic template maps, as described in Kogut et al. (1996a). The final result is equivalent to $T = \sum_i C^i_{\rm DMR} T^i_{\rm DMR} - 0.314 T_{\rm H} - 3.364 T_{\rm D}$, where $C^i_{\rm DMR}$ are the coefficients specified above, $T_{\rm H}$ is the Haslam map in K, and $T_{\rm D}$ is the DIRBE 140 μm map, in MJy sr^{-1}. The resulting map has units of μK, thermodynamic.

[c] Coefficients give the most sensitive combination of the 31, 53, and 90 GHz data, in thermodynamic units, consistent with the constraint that emission with a spectral index $\beta_{ff} = -2.15$ (free-free emission) be nullified. The channel maps are corrected for synchrotron and dust emission by subtracting best-fit Galactic template maps, as described in Kogut et al. (1996a). The final result is equivalent to $T = \sum_i C^i_{\rm DMR} T^i_{\rm DMR} + 0.170 T_{\rm H} - 2.055 T_{\rm D}$, where $C^i_{\rm DMR}$ are the coefficients specified above, $T_{\rm H}$ is the Haslam map in K, and $T_{\rm D}$ is the DIRBE 140 μm map, in MJy sr^{-1}. The resulting map has units of μK, thermodynamic.

The data are quantitatively tested for self-consistency by forming differences of the two-point functions and comparing them to simulations. The statistic for the test is defined as $\chi^2 = \Delta \boldsymbol{C}^T \cdot \boldsymbol{M}^{-1} \cdot \Delta \boldsymbol{C}$, where $\Delta \boldsymbol{C}$ is the observed difference between two-point functions, with entries $\Delta C_a = C_a^{(1)} - C_a^{(2)}$ (a denotes an angular separation bin, superscripts 1 and 2 denote specific data selections), and $\boldsymbol{M} = \langle (\Delta \boldsymbol{C})(\Delta \boldsymbol{C})^T \rangle$ is the covariance matrix computed from simulations. For each realization in the Monte Carlo, we generate a single realization of a scale-invariant power-law sky with unit normalization, and six noise maps, one per channel, with appropriate noise level and coverage (Bennett et al. 1996). We assume the noise is uncorrelated from pixel to pixel, based on the analysis of Lineweaver et al. (1994). It is then possible to generate an ensemble of simulated two-point functions for any desired auto- or cross-correlation function constructable from the DMR data. We generate such an ensemble for each of the six panels depicted in Figure 1; note that a given realization of the six combinations shares a common CMB signal. We compute χ^2 as defined above for each possible difference and compare its value to the ensemble derived from the simulations. Note that our computation of the covariance matrix from simulations automatically includes bin-bin correlations in the definition of χ^2. In no case does the observed value of χ^2 exceed the 5% confidence upper limit derived from the simulations, which corroborates the visual consistency of the data.

The two-point functions obtained from selected multifrequency combinations of the data are shown in Figure 2. We

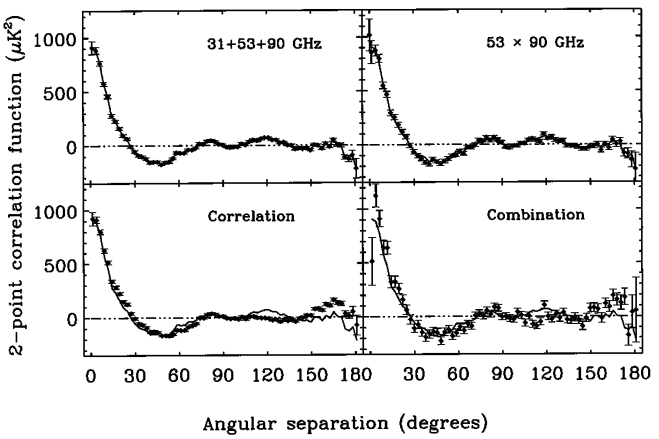

FIG. 2.—Two-point correlation functions obtained from the multifrequency maps after monopole and dipole subtraction. *Top left*: autocorrelation function of the weighted average map constructed from all six DMR channels. *Top right*: cross-correlation function of the 53 GHz weighted sum map with the 90 GHz weighted sum map. *Bottom left*: autocorrelation function of the weighted average map with best-fit Galaxy template maps subtracted from the map (Kogut et al. 1996a). *Bottom right*: autocorrelation function of the linear combination map designed to cancel free-free emission. This map has a best-fit model of the synchrotron and dust emission also subtracted. In all panels the error bars represent the uncertainty due to instrument noise, as described in the text. Zero-lag point in each of the autocorrelation functions is off-scale due to the noise contribution. To guide the eye, the solid line is the autocorrelation of the weighted average map (*top left panel*).

plot the autocorrelation of the weighted average map, the cross-correlation of the 53 and 90 GHz maps, and the autocorrelation of two maps which have had residual, high-latitude Galactic emission modeled and removed (Table 1 and Kogut et al. 1996a). Note the excellent consistency between the autocorrelation of the weighted average map, which is sensitive to *all* structure in that map, and the cross-correlation of the 53 and 90 GHz data, which is sensitive only to common structure in the maps. Note also that the two methods used to model and remove high-latitude Galactic emission introduce only small changes in the two-point data, and hence in the angular power spectrum. This observation, coupled with the fact that the correlation and combination model maps render very similar two-point functions, supports the claim of Kogut et al. (1996a) that the free-free emission at high latitudes is (1) weak, and (2) approximately traced by the DIRBE 140 μm map at 7° resolution.

3. QUADRUPOLE NORMALIZATION

Given a power-law model of initial Gaussian density fluctuations, $P(k) \propto k^n$, where $P(k)$ is the power spectrum of density fluctuations as a function of comoving wavenumber k, it is possible to derive the corresponding angular power spectrum of CMB fluctuations, $C_\ell = \langle |a_{\ell m}|^2 \rangle$ (Bond & Efstathiou 1987). The result is

$$C_\ell = C_2 \frac{\Gamma[\ell + (n-1)/2]\Gamma[(9-n)/2]}{\Gamma[\ell + (5-n)/2]\Gamma[(3+n)/2]} . \quad (2)$$

For the scale-invariant case, $n = 1$, this reduces to $C_\ell = 6C_2/[\ell(\ell+1)]$, which has one free parameter, the mean quadrupole moment C_2. We customarily express the normalization in terms of $Q_{\rm rms-PS} \equiv [(5/4\pi)C_2]^{1/2}$, the mean rms temperature fluctuation expected in the quadrupole component of the anisotropy. We determine the most likely quadrupole normalization, $Q_{\rm rms-PS}$, from the two-point function by evaluating the Gaussian approximation to the likelihood function

$$\mathcal{L}(Q_{\rm rms-PS}) \propto \frac{e^{-1/2\Delta C^T \cdot M^{-1} \cdot \Delta C}}{\sqrt{\det(M)}} . \quad (3)$$

Here ΔC^T and ΔC are row and column vectors with entries $\Delta C_a = C(\alpha_a) - \langle C(\alpha_a) \rangle$, $a = 0, \ldots 70$, and $M = \langle (\Delta C)(\Delta C)^T \rangle$ is the covariance matrix of the correlation function. The angle brackets denote averages over both measurement errors and over the ensemble of anisotropy fields implied by cosmic variance for a given C_ℓ. We estimate the mean correlation and covariance matrix as a function of $Q_{\rm rms-PS}$ using Monte Carlo simulations described above. The simulations account for all important aspects of our data processing including monopole and dipole (and quadrupole) removal on the cut sky. Because of this subtraction, the bins of a given correlation function are not all independent so the covariance matrices derived from the simulations are formally singular. We invert these matrices to form χ^2 using singular value decomposition, which permits an unambiguous identification of the zero modes that arise due to multipole subtraction. We then evaluate the logarithm of the likelihood, $\ln \mathcal{L} = -\frac{1}{2}\{\chi^2 + \ln[\det(M)] + \text{const.}\}$, in steps of 1 μK in $Q_{\rm rms-PS}$, spline the result to a resolution of 0.01 μK, and identify the maximum.

We test the likelihood method for accuracy by feeding the

TABLE 2

SCALE-INVARIANT POWER SPECTRUM NORMALIZATION

		$\ell_{\rm min} = 2^b$		$\ell_{\rm min} = 3^b$	
MAP 1[a]	MAP 2[a]	$Q_{\rm rms-PS}$ (μK)	χ^2	$Q_{\rm rms-PS}$ (μK)	χ^2
Single-Frequency Cross-Correlation					
31A	31B	18.2 ± 4.1	68.3	18.0 ± 4.6	71.0
53A	53B	18.3 ± 1.6	73.5	18.6 ± 1.7	69.6
90A	90B	16.4 ± 2.2	72.3	18.4 ± 2.3	71.0
Single-Frequency Autocorrelation					
31ws	31ws	17.1 ± 3.7	67.9	17.6 ± 4.0	79.6
53ws	53ws	18.7 ± 1.6	99.9	19.4 ± 1.6	97.5
90ws	90ws	17.5 ± 2.0	63.5	19.0 ± 2.2	61.5
Multifrequency Cross-Correlation					
53ws	90ws	17.2 ± 1.5	60.8	17.8 ± 1.5	64.1
53ss	90ss	17.0 ± 1.6	61.2	17.9 ± 1.6	62.3
Multifrequency Autocorrelation					
53 + 90	53 + 90	18.5 ± 1.4	84.2	19.6 ± 1.5	83.5
31 + 53 + 90 ...	31 + 53 + 90	18.6 ± 1.4	80.0	19.3 ± 1.4	78.2
Multifrequency Autocorrelation with Galaxy Model					
Correlation	Correlation	17.5 ± 1.4	76.2	18.5 ± 1.4	78.3
Combination....	Combination	16.7 ± 2.0	89.2	17.8 ± 2.2	92.4

[a] Coefficients that comprise the map combinations in these columns are given in Table 1, except for 53ss and 90ss, which are straight sum maps: (A + B)/2.

[b] $\ell_{\rm min}$ is the lowest order multipole remaining in the map after subtracting a best-fit multipole of order $\ell_{\rm min} - 1$. $Q_{\rm rms-PS}$ is the most likely quadrupole normalization, after calibrating the likelihood with Monte Carlo simulations. χ^2 is tabulated, for reference, with respect to the mean of a scale-invariant model with the corresponding most likely normalization.

simulated two-point functions into the likelihood function and solving for an ensemble of $Q_{\rm rms-PS}$ maxima. We define the bias in our method to be $\Delta Q = \langle Q_{\rm max} \rangle - Q_{\rm in}$, where $\langle Q_{\rm max} \rangle$ is the mean of the recovered maxima and $Q_{\rm in}$ is the simulation input normalization. The resulting bias depends on the noise level in the data, but ranges from -0.2 to -0.4 μK for the all the cases except the 31 GHz data where it is ~ -1 μK. We correct for this bias in all reported results. The uncertainty we assign to $Q_{\rm rms-PS}$ is the rms scatter of the ensemble $Q_{\rm max}$, which typically exceeds the rms of the Gaussian likelihood by about 10%.

The corrected power spectrum normalization deduced from a variety of data combinations is given in Table 2. The smallest and largest normalization deduced from any data combination are 16.4 and 19.6 μK, respectively, with values ~ 18 μK generally preferred. The normalization inferred from the two-point function is now in better agreement with other determinations than was the case with the 2 yr data (Bennett et al. 1994). The change is due to data selection: with the 2 yr data, we only analyzed the 53×90 GHz cross-correlation function; with the 4 yr data we have analyzed many more data combinations, including the autocorrelation of a weighted average multifrequency map which yields a normalization ~ 1.5 μK higher than the cross-correlation. The multifrequency autocorrelation is more comparable to the data analyzed by other methods, and the two-point analysis yields consistent results in that case. For a comparison, see Table 2 of Bennett et al. (1996). In general, the normalization inferred from the 4 yr data is slightly less than we found after 2 yr, in part because of the extension of the Galaxy cut. For comparison, the 31 + 53 + 90 GHz autocorrelation with a straight 20° cut yields a best-fit normalization of $Q_{\rm rms-PS} = 19$ μK. As shown in Table 2, the effects of further modeling and subtraction of Galactic emission are less than 1 μK in the normalization.

While a likelihood analysis is capable of inferring the best-fit parameters for a given model, it does not say anything per se about the goodness of fit. For reference we have included in Table 2 the values of χ^2 at the maximum likelihood value of $Q_{\rm rms-PS}$ (with $n = 1$). Since the two-point function is only approximately multivariate Gaussian distributed, our tabulated statistic is only approximately χ^2 distributed. However, we have used our Monte Carlo simulations to compute the expected distribution of this statistic and find it to be approximately χ^2 with a mean of ~ 70 and a standard deviation of ~ 12. The values computed with the DMR data are very consistent with this distribution, implying that the data are well fit by a scale-invariant power spectrum.

Analyses of $Q_{\rm rms-PS|n=1}$ have also been reported by Górski et al. (1996), Hinshaw et al. (1996), Kogut et al. (1996b), and Wright et al. (1996). All results lie between 16.4 and 19.6 μK, with most between 17.5 and 18.5 μK. In general, all *methods* for analyzing a given data combination give consistent results, while there is modest dependence on data selection. Fortunately, this dependence does not exceed the statistical uncertainty due to cosmic variance and instrument noise. Based on our judgment, a reasonable value for the normalization of a scale-invariant spectrum is $Q_{\rm rms-PS|n=1} = 18 \pm 1.6$ μK, where the quoted error is slightly dilated, relative to the statistical error, to encompasses the range of normalizations observed in different data subsets.

We gratefully acknowledge the many people who made this paper possible: the NASA Office of Space Sciences, the *COBE* flight operations team, and all of those who helped process and analyze the data. We thank our referee, Ken Ganga, for comments that helped improve the clarity of this paper.

REFERENCES

Bennett, C. L., et al. 1992, ApJ, 396, L7
———. 1994, ApJ, 436, 423
———. 1996, ApJL, 464, L1
Bond, J. R., & Efstathiou, G. 1987, MNRAS, 226, 655
Górski, K. M., Banday, A. J., Bennett, C. L., Hinshaw, G., Kogut, A., Smoot, G. F., & Wright, E. L. 1996, ApJL, 464, L11
Górski, K. M., Hinshaw, G., Banday, A. J., Bennett, C. L., Wright, E. L., Kogut, A., Smoot, G. F., & Lubin, P. 1994, ApJ, 430, L89
Hinshaw, G., Banday, A. J., Bennett, C. L., Górski, K. M., Kogut, A., Smoot, G. F., & Wright, E. L. 1996a, ApJL, 464, L17
Kogut, A., Banday, A. J., Bennett, C. L., Górski, K. M., Hinshaw, G., Smoot, G. F., & Wright, E. L. 1996a, 464, L5
Kogut, A., Banday, A. J., Bennett, C. L., Górski, K. M., Hinshaw, G., Smoot, G. F., & Wright, E. L. 1996b, 464, L29
Kogut, A., et al. 1992, ApJ, 401, 1
Lineweaver, C. H., et al. 1994, ApJ, 436, 452
Smoot, G. F., et al. 1992, ApJ, 396, L1
Wright, E. L., et al. 1992, ApJ, 396, L13
Wright, E. L., Bennett, C. L., Górski, K. M., Hinshaw, G., & Smoot, G. F. 1996, ApJL, 464, L21
Wright, E. L., Smoot, G. F., Bennett, C. L., & Lubin, P. M. 1994a, ApJ, 436, 443
Wright, E. L., Smoot, G. F., Kogut, A., Hinshaw, G., Tenorio, L., Lineweaver, C., Bennett, C. L., & Lubin, P. M. 1994b, ApJ, 420, 1